Available online at www.sciencedirect.com
SCIENCE DIRECT®
Journal of Sound and Vibration 291 (2006) 437–461
JOURNAL OF SOUND AND VIBRATION
www.elsevier.com/locate/jsvi

Design of robust controllers and a nonlinear observer for the control of a single-link flexible robotic manipulator

N.G. Chalhoub*, G.A. Kfoury, B.A. Bazzi

Department of Mechanical Engineering, Wayne State University, Detroit, MI 48202, USA

Received 23 August 2004; received in revised form 31 May 2005; accepted 16 June 2005
Available online 25 August 2005

Abstract

Two robust nonlinear controllers along with a nonlinear observer have been developed in this study to control the rigid and flexible motions of a single-link robotic manipulator. The controllers and the observer have been designed based on a simplified model of the arm, which only accounts for the first elastic mode of the beam. The controllers consist of a conventional sliding mode controller (CSMC) and a fuzzy-sliding mode controller (FSMC). Moreover, the robust nonlinear observer has been designed based on the sliding mode methodology.

The dynamic model, used in assessing the performances of the controllers and the observer, considers the first two elastic modes of the beam. The inclusion of the second elastic mode has been done to investigate the effects of unstructured uncertainties on the overall performance of the closed-loop system. The digital simulations have demonstrated the capability of the observer in yielding accurate estimates of the state variables in the presence of modeling uncertainties. Moreover, they served to prove the viability of using the observer to provide on-line estimates of the state variables for the computation of the control signals. The results have illustrated robust performances of the controllers and the observer in controlling the rigid and flexible motions of the manipulator in the presence of both structured and unstructured uncertainties. This was achieved irrespective of the differences in the initial conditions between the plant and the observer.

Furthermore, the structural deformations, incurred by the beam at the onset of its movement, have been shown to be significantly reduced by fuzzy-tuning the η-control parameter. The results have demonstrated the superiority of the FSMC over the CSMC in producing less oscillatory and more accurate response of

*Corresponding author. Tel.: +1 313 577 3753; fax: +1 313 577 8789.
E-mail address: nchalhoub@eng.wayne.edu (N.G. Chalhoub).

0022-460X/$ - see front matter
doi:10.1016/j.jsv.2005.06.019

Nomenclature

A	cross sectional area of the beam
E	Young's modulus of elasticity
$\bar{g}$	$(q(t), \dot{q}(t))$ vector representing the right-hand side of the equations of motion excluding the control terms
I	moment of inertia of the cross sectional area of the beam
(I, J, K)	inertial reference frame fixed at point O
$(\tilde{i}, \tilde{j}, \tilde{k})$	non-inertial, body fixed, rotating reference frame
L	length of the compliant beam
$M(x)$	inertia matrix
M_B	mass of the beam
m_P	mass of the payload
$q_{2i}(t)$	generalized coordinate for the ith elastic mode of the beam in the horizontal transverse direction
s_o	sliding surface evaluated at $t = 0$, $s(e(t = 0), t = 0)$
s_{ob}	sliding surface used in the observer design
t_{reach}	time at which the system trajectory reaches the sliding surface
w	weighing factor dependent on the fuzzy term α
ρ	density of aluminum
θ	angular displacement at the base joint of the beam
θ_d	desired angular displacement at the base joint of the beam
$()_e$	"e" subscript denotes an estimated value of the state variable

the angular displacement at the base joint, in damping out the unwanted vibrations of the beam, and in requiring significantly smaller control torques.

1. Introduction

The poor end effector positional accuracy of flexible robotic manipulators has limited their applications to tasks that are error tolerant. The positional inaccuracies stem from both tracking errors and structural deflections of the robot. Therefore, the controller objective is to yield good tracking characteristic of the robot while actively damping out the unwanted vibrations of the links. To achieve this goal, many researchers have developed control schemes that have led to a significant reduction in the vibrations of the arm by finding a compromise between the positional accuracy of the end effector and the high-speed operation of the robot [1–5]. However, most of these controllers are not robust to external disturbances and modeling uncertainties.

The current study focuses on the sliding mode methodology [6–8] for the development of robust controllers and an observer to control a single-link flexible robotic manipulator. Numerous sliding mode controllers (SMC) have been proposed in the literature to address the tracking problem for multi-link rigid robotic manipulators [9–12] and single-link flexible robot arms [13–15]. The different versions were introduced to address the shortcomings of the SMC. For instance, if the starting point of the system trajectory is located off the sliding surface then there will be a reaching period during which the system is vulnerable to parameter variations and external disturbances.

Choi et al. [16] proposed an SMC with a stepwise moving sliding surface (MSS) for a class of second-order uncertain systems. Choi and Park [11] implemented this technique on a two-degree-of-freedom rigid robotic manipulator. Ha et al. [12] modified the approach of Choi et al. [16] by using continuous functions for the coefficients of the MSS. Bartoszewicz [17] addressed the shortcomings of these controllers [12,16] by suggesting a control algorithm that prevents the system's representative point from leaving the MSS; thus, ensuring the robustness of the controlled system during the reaching phase.

Kim and Inman [18] used a CSMC to damp out the vibrations of a flexible cantilevered beam with piezoelectric actuators/sensors. No rigid-body motion is considered in this study. The CSMC is coupled in this study with a nonlinear sliding mode observer to eliminate the effects of observation spillover in the control of flexible structures.

Other studies attempted to combine the salient features of fuzzy logic and sliding mode control theory by fuzzy-tuning the parameters of the SMC [8,10,12]. Choi and Kim [10] designed a fuzzy-sliding mode controller (FSMC) for a two-link rigid robotic manipulator by replacing the feedback gains and their corresponding signum functions in the CSMC control law by time-varying terms that were determined by a fuzzy logic inference system. Their results demonstrated the superiority of FSMC over CSMC in improving the tracking accuracy and in attenuating the chattering in the control signals.

Similarly, Choi et al. [13] used a sliding mode controller with an MSS to regulate the tip position of a single-link flexible manipulator. Linear time-invariant equations of motion are used to describe the rigid and flexible motions of the flexible link. Their results demonstrate that the sliding mode controller with MSS can yield a better performance than the CSMC in regulating the vibrations of the beam.

It should be pointed out that SMC rely on the availability of the state variables of the system for the computation of their control actions. Therefore, a robust observer is needed to yield accurate estimates of the state variables in the presence of both parametric uncertainties and external disturbances.

The variable structure systems (VSS) theory has been successfully used in the development of robust observers for dynamical systems with bounded nonlinearities and/or uncertainties [19–21]. These observers do not require exact knowledge of the plant parameters and/or nonlinearities. Their design is solely based on knowing the upper bounds of the system uncertainties and/or nonlinearities.

Walcott and Zak [19] developed a variable structure observer for systems with observable linear parts and bounded nonlinearities and/or uncertainties. Wagner and Shoureshi [22] demonstrated that Walcott and Zak's observer [19] yields estimates of the state variables that have faster convergence rates and smaller steady-state errors than those generated by Baumann and Rugh's [23], and Thau's [24] nonlinear observers.

Slotine et al. [20] discussed in detail the design procedure of VSS observers for nonlinear systems expressed in the companion form. Furthermore, they provided a general guidance on how to determine the gains of sliding mode observers for nonlinear systems expressed in the general form. This methodology has been used by Canudas De wit and Slotine [25] in designing a nonlinear sliding mode observer to estimate the angular velocity at the joints for a rigid robotic manipulator.

In this study, two robust nonlinear controllers along with a nonlinear observer have been developed to control the rigid and flexible motions of a single-link robotic manipulator. The controllers consist of a conventional sliding mode controller (CSMC) and an FSMC. The FSMC has been proposed herein to enhance the tracking characteristic and vibration suppression

capability of the CSMC. In the proposed FSMC, the η control parameter has been fuzzy-tuned in order to reduce the structural deformations that are attributed to the whiplash effect. Furthermore, the new FSMC design entails the use of two Lyapunov functions that enables the sliding mode controller to exert a negative control torque during the period when the system is approaching the boundary layer neighboring the sliding surface. This will significantly reduce the momentum with which the system approaches the boundary layer; thus, resulting in considerably smaller structural deformations of the system. In addition, a robust nonlinear observer, based on the sliding mode methodology [20], has been designed to yield accurate estimates of the state variables in the presence of model uncertainties and difference in the initial conditions between the estimator and the plant.

The dynamic model, capturing the rigid and flexible motions of a single-link robotic manipulator, is derived in Section 2. Subsequently, both the CSMC and the FSMC are designed in Section 3. Moreover, the design of the nonlinear observer is included in Section 4. The combined performances of the controllers and the observer are assessed in Section 5. Finally, the work is summarized and its main contributions are highlighted.

2. Dynamic model

The physical system consists of a flexible link connected to a revolute joint (see Fig. 1). The beam is made of aluminum and has an annular cross section. It is restricted in its motion to the horizontal plane. The stiffness of the beam in the longitudinal direction is much higher than in flexure. Therefore, only the in-plane transverse deflection of the beam, $W(x,t)$, is considered in addition to its rigid-body motion. The payload consists of a lumped mass mounted at the free-end of the beam.

The dynamic model retains all the coupling terms between the rigid and flexible motions of the beam. The position vector of an arbitrary point on the flexible link is given by

$$\underset{\sim}{r}_B = x\,\underset{\sim}{i} + W(x,t)\,\underset{\sim}{j}, \tag{1}$$

where x is the time invariant since the longitudinal vibration is neglected (see Fig. 1). The assumed modes method is implemented to approximate $W(x,t)$, which is considered here to be dominated

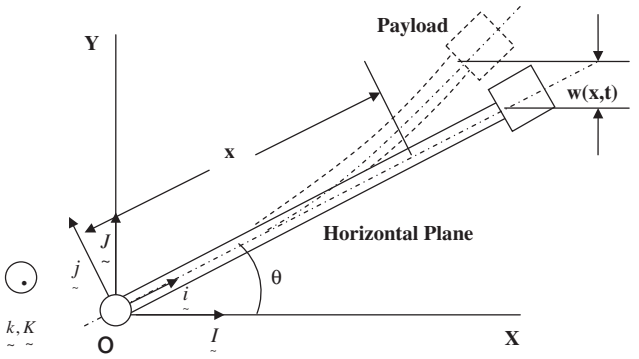

Fig. 1. Flexible link geometry and coordinates.

by the first two elastic modes [26]. It is written as a linear combination of admissible functions, $\Phi_i(x)$, of spatial coordinate, and time-dependent generalized coordinates, $q_{2i}(t)$. The admissible functions are chosen to be the first two eigenfunctions of a clamped-free beam derived based on the Euler–Bernoulli beam assumption [27]. Similarly, the position vector of the payload is determined by substituting x by L in Eq. (1). The velocity vector of an arbitrary point of the beam is given by

$$\underset{\sim}{\dot{r}}_B = \underset{\sim}{\dot{r}}_B|_{(\underset{\sim}{i},\underset{\sim}{j},\underset{\sim}{k})} + \underset{\sim}{\omega} \times \underset{\sim}{r}_B, \tag{2}$$

where $\underset{\sim}{\omega}$ is equal to $\dot{\theta}\,\underset{\sim}{k}$. The total kinetic energy of the system is written as

$$T_t = \frac{1}{2}\int_{M_B} (\underset{\sim}{\dot{r}}_B \cdot \underset{\sim}{\dot{r}}_B)\,\mathrm{d}m + \frac{1}{2} m_p (\underset{\sim}{\dot{r}}_p \cdot \underset{\sim}{\dot{r}}_p). \tag{3}$$

The strain energy stored in the system is expressed as

$$E_t = \frac{1}{2}\int_0^L EI\left(\frac{\partial^2 W(x,t)}{\partial x^2}\right)^2 \mathrm{d}x. \tag{4}$$

The total virtual work, done on the system, is determined as follows:

$$\delta W_t = \tau_1 \delta\theta + \frac{1}{2}\int_0^L P(\dot{\theta}, x)\left(\frac{\partial W(x,t)}{\partial x}\right)^2 \mathrm{d}x, \tag{5}$$

where τ_1 is the non-conservative generalized control torque applied at the base joint. The second term reflects the stiffening effect of the beam induced by the centrifugal force $P(\dot{\theta}, x)$ [3,26,28], which can be expressed as

$$P(\dot{\theta}, x) = \frac{1}{2}\rho A \dot{\theta}^2 L^2\left(1 - \frac{x^2}{L^2}\right) + m_P L \dot{\theta}^2. \tag{6}$$

Note that the variation of the inertial axial force, $P(\dot{\theta}, x)$, due to the flexible motion is neglected in this formulation.

The equations governing the rigid and flexible motions of the beam are obtained by implementing the Lagrange principle. The resulting equations of motion are three highly nonlinear, coupled, stiff, second-order ordinary differential equations. These equations are then converted to a set of six first order ordinary differential equations that can be written as

$$\begin{pmatrix} \dot{x}_1(t) \\ \dot{x}_2(t) \\ \dot{x}_3(t) \\ \dot{x}_4(t) \\ \dot{x}_5(t) \\ \dot{x}_6(t) \end{pmatrix} = \begin{pmatrix} f_1(\underset{\sim}{x}(t), \tau_1) \\ f_2(\underset{\sim}{x}(t), \tau_1) \\ f_3(\underset{\sim}{x}(t), \tau_1) \\ f_4(\underset{\sim}{x}(t), \tau_1) \\ f_5(\underset{\sim}{x}(t), \tau_1) \\ f_6(\underset{\sim}{x}(t), \tau_1) \end{pmatrix} = \begin{pmatrix} x_4(t) \\ x_5(t) \\ x_6(t) \\ -M^{-1}(\underset{\sim}{x}(t)) \begin{bmatrix} \bar{g}_1(\underset{\sim}{x}(t)) + \tau_1 \\ \bar{g}_2(\underset{\sim}{x}(t)) \\ \bar{g}_3(\underset{\sim}{x}(t)) \end{bmatrix} \end{pmatrix}, \tag{7}$$

where the state vector is defined to be $x(t) = [\theta \quad q_{21} \quad q_{22} \quad \dot{\theta} \quad \dot{q}_{21} \quad \dot{q}_{22}]^{\mathrm{T}}$. The state equations are solved numerically by using the Gear's method [29], which is well suited for solving stiff systems. This model is used, in this study, as a test bed for assessing the combined performances of the controllers and the observer in the presence of both structured and unstructured uncertainties of the plant.

However, it should be emphasized that a simplified version of the model, obtained by ignoring the second elastic mode of the beam, has been used herein in the design of the controllers and the observer. Its equations can be expressed as

$$\dot{\underset{\sim}{x}}_r = \begin{pmatrix} f_{r1}(\underset{\sim}{x}_r, \tau_1) \\ f_{r2}(\underset{\sim}{x}_r, \tau_1) \\ f_{r3}(\underset{\sim}{x}_r, \tau_1) \\ f_{r4}(\underset{\sim}{x}_r, \tau_1) \end{pmatrix} = \begin{pmatrix} x_{r3} \\ x_{r4} \\ -M_r^{-1}(\underset{\sim}{x}_r)\begin{bmatrix} \bar{g}_{r1}(\underset{\sim}{x}_r) + \tau_1 \\ \bar{g}_{r2}(\underset{\sim}{x}_r) \end{bmatrix} \end{pmatrix} = \begin{pmatrix} x_{r3} \\ x_{r4} \\ g_{r1}(\underset{\sim}{x}_r) + b_1(\underset{\sim}{x}_r)\tau_1 \\ g_{r2}(\underset{\sim}{x}_r) + b_2(\underset{\sim}{x}_r)\tau_1 \end{pmatrix}, \tag{8}$$

where $\underset{\sim}{x}_r = [\theta \quad q_{21} \quad \dot{\theta} \quad \dot{q}_{21}]^{\mathrm{T}}$. Note that $M_r(\underset{\sim}{x}_r)$, $\bar{g}_{r1}(\underset{\sim}{x}_r)$ and $\bar{g}_{r2}(\underset{\sim}{x}_r)$ are obtained from $M(\underset{\sim}{x})$, $\bar{g}_1(\underset{\sim}{x})$ and $\bar{g}_2(\underset{\sim}{x})$ in Eq. (7) by deleting the entries and terms associated with $q_{22}(t)$ and its time derivative. The detailed expressions for f_{r3} and f_{r4} are listed in Appendix A.

3. Design of the robust nonlinear controllers

Two robust controllers, consisting of a CSMC and an FSMC, have been designed in this study to control the rigid and flexible motions of the single-link robotic manipulator. Their objective is to provide a robust set-point tracking characteristic of the flexible manipulator while actively damping out the unwanted vibrations.

Both controllers are designed based on the following θ equation:

$$\ddot{\theta} = \dot{x}_{r3} = g_{r1}(\underset{\sim}{x}_r) + b_1(\underset{\sim}{x}_r)\tau_1. \tag{9}$$

The term $b_1(\underset{\sim}{x}_r)$ is considered to be fully known. However, $g_{r1}(\underset{\sim}{x}_r)$ is treated as an unknown term. It has been approximated by the following nominal function $\hat{g}_{r1}$:

$$\hat{g}_{r1}(\underset{\sim}{\hat{x}}_r) = \frac{-\hat{x}_{r2}(700\hat{x}_{r3}\hat{x}_{r4} - 70\hat{x}_{r3} - 770,000)}{300\hat{x}_{r2}^2 + 6}. \tag{10}$$

Note that the nominal functions, used in this study, are generated by randomly changing the numerical values of all the coefficients as well as the exponents of some of the terms in their respective exact functions. The rationale is to introduce structured uncertainties in the closed-loop system.

Only the upper bound of the model imprecision is assumed to be known. It is defined as

$$|\Delta f_{r3}| = |f_{r3} - \hat{f}_{r3}| = |g_{r1} - \hat{g}_{r1}| \leqslant F_3. \tag{11}$$

Since the task of the controller is to force θ to track the desired angular displacement, θ_d, then the tracking error is defined to be

$$e_1 = x_{r1} - x_{r1d} = \theta - \theta_d. \tag{12}$$

Accordingly, the sliding surface is expressed as

$$s(\underset{\sim}{e}, t) = \dot{e}_1 + \lambda e_1. \tag{13}$$

Based on the nominal function $\hat{g}_{r1}$ of the system, the continuous control law $\tau_{1\text{eq}}$, satisfying $\dot{s}(\underset{\sim}{e}, t) = 0$, is expressed as

$$\tau_{1\text{eq}} = b_1^{-1}\{-\hat{g}_{r1} + \ddot{x}_{1d} - \lambda \dot{e}_1\}. \tag{14}$$

Once on the surface, the dynamic response of the system is governed by

$$\left(\frac{\mathrm{d}}{\mathrm{d}t} + \lambda\right) e_1 = 0. \tag{15}$$

The tracking error will be driven to zero by selecting λ to be a strictly positive constant. To force the system trajectory to converge to the sliding surface in the presence of both model uncertainties and disturbances, the feedback control torque τ_1 is defined as

$$\tau_1 = \tau_{1\text{eq}} - b_1^{-1} k \,\mathrm{sgn}(s), \tag{16}$$

where k is determined by satisfying the following sliding condition:

$$\frac{\mathrm{d}}{\mathrm{d}t} V_1 = \frac{1}{2}\frac{\mathrm{d}}{\mathrm{d}t} s^2(\underset{\sim}{e}, t) \leqslant -\eta |s|. \tag{17}$$

Note that $V_1 = \frac{1}{2}s^2$ is a positive definite function. It represents the squared distance between the sliding surface and any representative point of the system. The selection of η to be strictly positive will ensure that $\dot{V}_1$ is negative definite. Therefore, V_1 becomes a Lyapunov function that decreases along all trajectories of the system; thus, causing the sliding surface to become an invariant set. It can be easily proven that the above inequality is satisfied by selecting k to be

$$k \geqslant \eta + F_3. \tag{18}$$

To alleviate the chattering problem induced by the switching term in the control signal, the sgn(s) term in Eq. (16) is often replaced by a saturation function as follows:

$$\tau_1 = \tau_{1\text{eq}} - b_1^{-1} k \,\mathrm{sat}\left(\frac{s}{\Phi}\right), \tag{19}$$

where Φ is the thickness of the boundary layer. It is considered herein to be time-variant. Therefore, to ensure convergence of the system trajectory to the boundary layer, the sliding condition in Eq. (17) had to be modified to the following form:

$$\frac{1}{2}\frac{\mathrm{d}}{\mathrm{d}t} s^2(\underset{\sim}{e}, t) \leqslant (\dot{\Phi} - \eta)|s|. \tag{20}$$

The above condition can be satisfied by changing the expression of τ_1 as follows:

$$\tau_1 = \tau_{1\text{eq}} - b_1^{-1} \bar{k} \,\mathrm{sat}\left(\frac{s}{\Phi}\right), \tag{21}$$

where $\bar{k} = k - \dot{\Phi}$. The differential equation governing the behavior of $\dot{\Phi}$ is derived in detail in the literature [6,7]. It is given by

$$\dot{\Phi} + \lambda\Phi = k(\theta_d), \tag{22}$$

where $k(\theta_d)$ is defined in Eq. (18).

Up to this stage, the formulation has only dealt with the design of the CSMC. To enhance the performance of this controller, its parameter η is now fuzzy-tuned. The rationale is to reduce both the rise time and the oscillations of θ, to attenuate the deformations at the onset of the beam movement, and to require a relatively smaller control torque. This is done by designing the η-fuzzy inference system (FIS) to assign small numerical values to η at the beginning of the beam movement. The rationale is to gradually build up the momentum of the beam in order to reduce the "whiplash" effect; thus, reducing the deformations at the onset of the beam movement. Once the beam is set in motion, η is increased considerably in order to shorten the reaching time to the sliding patch. In the vicinity of the sliding surface, η is once again reduced significantly in order to decrease the thickness of the boundary layer Φ, whose steady-state value is directly proportional to η. It should be pointed out that small values of Φ are desired when the system is nearing the sliding surface in order to improve its tracking accuracy.

The input to the η-FIS is selected to be the normalized error in the base joint angular displacement, $e_n = (\theta_d - \theta)/\theta_d$. Note that the normalized value is used to adapt the FIS to any range of the error input. The membership functions for the input and output variables of the η-FIS are shown in Fig. 2. Furthermore, the fuzzy rule base consists of five linguistic "if-then" rules that are summarized in Table 1. The Mamdani-type FIS is used herein to compute the centroid of the resulting fuzzy set in order to defuzzify the output into a crisp value for η.

Furthermore, it should be stressed that the CSMC is unable to exert a negative control torque during the reaching phase. As a consequence, the system reaches the sliding surface with a large momentum and a sharp angle of approach causing its response to be highly oscillatory inside the boundary layer. The first few peaks will be truncated due to the robustness characteristic of the controller that prevents the system from exiting the boundary layer. However, the high control activity within the boundary layer results in a violently switching control torque that has a tendency to excite the elastic modes of the flexible structure. Thus, the structure of the CSMC had to be modified in this study to provide the controller with the capability of slowing down the system response prior to reaching the sliding patch. This is done by implementing the following positive definite function:

$$V_2 = \tfrac{1}{2}[s(1 + we_1^2)]^2. \tag{23}$$

It should be mentioned that the control signal, based on V_2, is only activated when the percentage $(s_o - s)/s_o \times 100$ is between 33% and 2%. Otherwise, the control scheme, based on V_1 in Eq. (21), is used. The sliding condition corresponding to V_2 can be written as

$$\frac{\mathrm{d}}{\mathrm{d}t}V_2 = \frac{1}{2}\frac{\mathrm{d}}{\mathrm{d}t}[s(1 + we_1^2)]^2 \leqslant [\dot{\Phi} - \eta](1 + we_1^2)^2|s|, \tag{24}$$

where $\eta > 0$ and $\bar{k}$ associated with the above condition is determined to be

$$\bar{k} \geqslant \eta - \dot{\Phi} + F + |s|\frac{\mathrm{d}[\ln(1 + we_1^2)]}{\mathrm{d}t}. \tag{25}$$

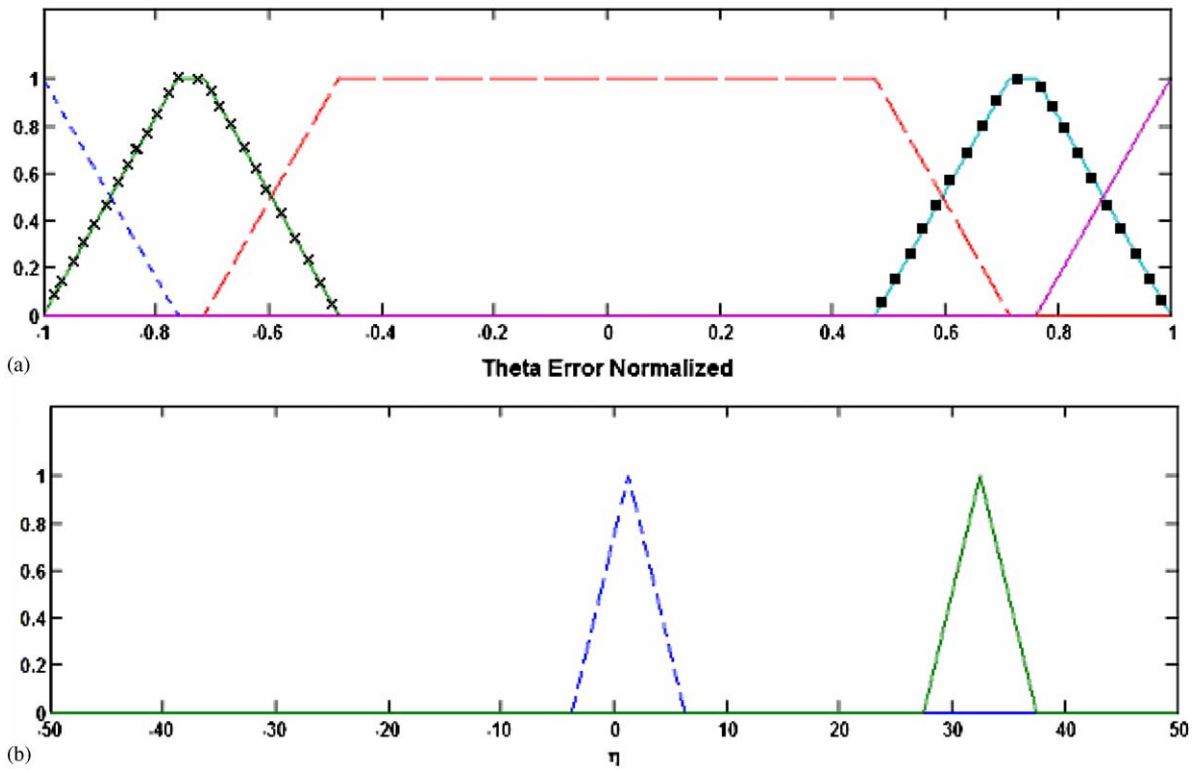

Fig. 2. Membership functions used in the η-FIS: (a) NLarge (- - - -), NSmall (⁎⁎⁎⁎), Zero (– – – –), PSmall (▪-▪-▪-▪), PLarge (——), (b) small (- - - -), large (——).

Table 1
Summary of the rules used in the η-FIS

Theta error normalized	η
NLarge	Small
NSmall	Large
Zero	Small
PSmall	Large
PLarge	Small

One approach to assign a negative control torque, during the reaching phase, is to force $\bar{k}$ to take on negative values. This is done herein as follows:

$$\alpha \geqslant \bar{k} \geqslant \eta - \dot{\Phi} + F + |s| \frac{[\dot{w}e_1^2 + 2e_1\dot{e}_1 w]}{(1 + we_1^2)}, \tag{26}$$

where $\alpha \leqslant 0$. Its value is assigned by an α-FIS, whose rules have been constructed to yield an appropriate negative control torque in the region nearing the sliding patch. The rationale is to dissipate most of the momentum of the system before it reaches the sliding surface. The input to the α-FIS is selected to be the normalized s, $s_n = (s_o - s)/s_o$, where s_o is equal to s when it is evaluated at $t = 0$. Note that s_n is used to adapt the FIS to arbitrary initial conditions of s_o. The membership functions for the input and output variables of the α-FIS are shown in Fig. 3. Furthermore, the fuzzy rule base consists of five linguistic "if-then" rules that are summarized in Table 2. The Mamdani-type FIS is used herein to compute the centroid of the resulting fuzzy set in order to defuzzify the output into a crisp value for α.

Next, both w and $\dot{w}$ of Eq. (26) have to be selected based on the assigned value of α while ensuring that the sliding condition of Eq. (24) is satisfied. This results in $\dot{V}_2$ being negative semi-definite. Thus, to achieve this goal, Eq. (26) is rearranged to yield

$$\dot{w} \leqslant \frac{1}{|s|e_1^2}(\alpha - \eta + \dot{\Phi} - F)(1 + we_1^2) - \frac{2\dot{e}_1 w}{e_1}. \tag{27}$$

The above equation along with the result of its numerical integration yields the numerical values for both w and $\dot{w}$ that are needed for the computation of $\bar{k}$ in Eq. (25).

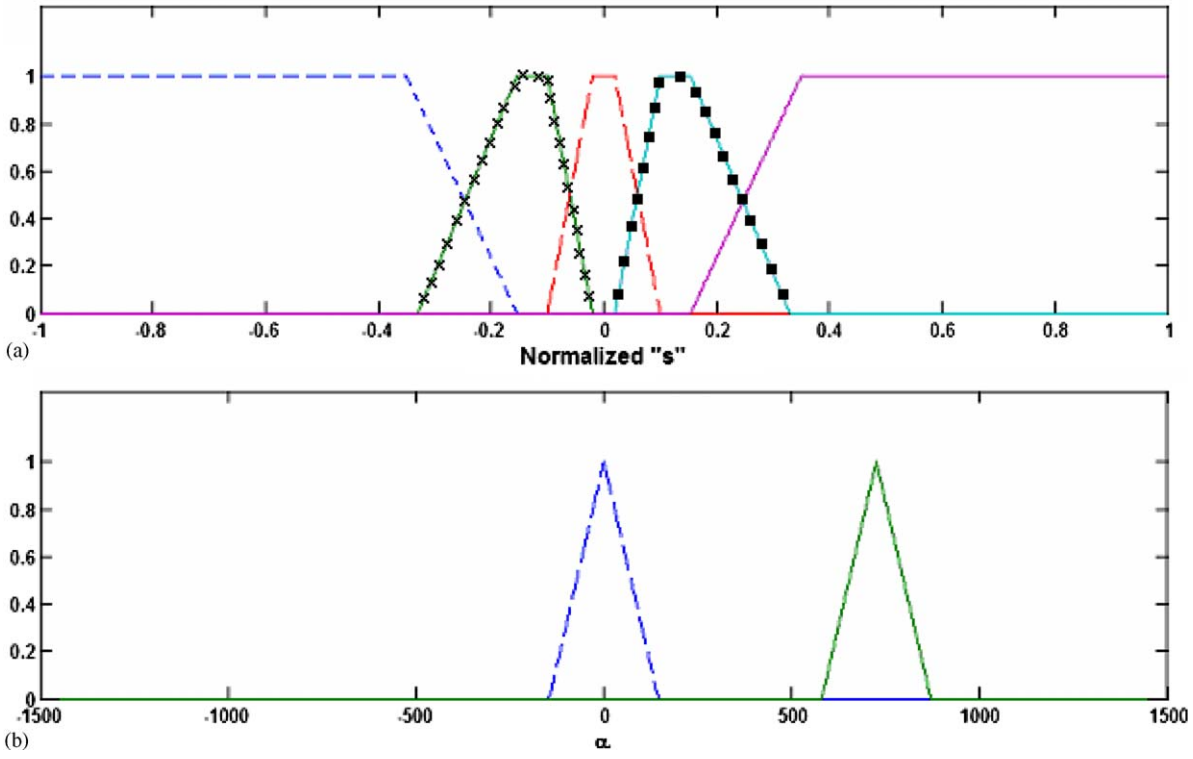

Fig. 3. Membership functions used in the α-FIS: (a) NLarge (- - - -), NSmall (⁎⁎⁎⁎), Zero (– – – –), PSmall (•–•–•), PLarge (——), (b) zero (- - - -), large (——).

Table 2
Summary of the rules used in the α-FLC

Normalized "s"	α
NLarge	Zero
NSmall	Large
Zero	Zero
PSmall	Large
PLarge	Zero

4. Design of the nonlinear robust observer

The objective of the observer is to accurately estimate θ, $q_{21}, \dot{\theta}$ and $\dot{q}_{21}$ in the presence of disturbances and model uncertainties. It is designed based on the simplified version of the model, which is defined in Eq. (8). The estimation error vector $\tilde{x}_r$ is determined from $\hat{x}_r - x_r = [\,\theta_e - \theta \quad q_{21e} - q_{21} \quad \dot{\theta}_e - \dot{\theta} \quad \dot{q}_{21e} - \dot{q}_{21}\,]^{\mathrm{T}}$. Both b_1 and b_2 are assumed to be fully known in the design of the observer. However, g_{r1} and g_{r2} are approximated by $\hat{g}_{r1}$ and $\hat{g}_{r2}$, respectively. Note that $\hat{g}_{r1}$ has already been defined in Eq. (10). However, $\hat{g}_{r2}$ is expressed as follows:

$$\hat{g}_{r2}(\underset{\sim}{\hat{x}}_r) = \frac{-\hat{x}_{r2}(650000\hat{x}_{r2}^2 + 60\hat{x}_{r2}\hat{x}_{r3}^2 - 780\hat{x}_{r4} + 80\hat{x}_{r3} + 930000)}{300\hat{x}_{r2}^2 + 6}. \tag{28}$$

Moreover, since only $\theta(t)$ is considered to be known from measurements in the design of the observer then the sliding surface is selected to be

$$s_{\mathrm{ob}} \triangleq \tilde{x}_{r1} = \hat{x}_{r1} - x_{r1}. \tag{29}$$

The state equations of the estimator are written as [20]:

$$\dot{\hat{x}}_{r1} = \hat{x}_{r3} - \bar{k}_1\tilde{x}_{r1} - k_1\,\mathrm{sgn}(\tilde{x}_{r1}), \tag{30a}$$

$$\dot{\hat{x}}_{r2} = \hat{x}_{r4} - \bar{k}_2\tilde{x}_{r1} - k_2\,\mathrm{sgn}(\tilde{x}_{r1}), \tag{30b}$$

$$\dot{\hat{x}}_{r3} = \hat{f}_{r3} - \bar{k}_3\tilde{x}_{r1} - k_3\,\mathrm{sgn}(\tilde{x}_{r1}), \tag{30c}$$

$$\dot{\hat{x}}_{r4} = \hat{f}_{r4} - \bar{k}_4\tilde{x}_{r1} - k_4\,\mathrm{sgn}(\tilde{x}_{r1}). \tag{30d}$$

Consequently, the estimation error vector equation is given by

$$\dot{\underset{\sim}{\tilde{x}}}_r = \Delta\underset{\sim}{f}_r - \bar{k}\tilde{x}_{r1} - k\,\mathrm{sgn}(\tilde{x}_{r1}), \tag{31}$$

where $\Delta f_r = [\,\tilde{x}_{r3} \quad \tilde{x}_{r4} \quad \Delta f_{r3} \quad \Delta f_{r4}\,]^{\mathrm{T}}$. Note that the modeling uncertainties Δf_{r3} and Δf_{r4} are determined from $(\hat{f}_{r3} - f_{r3})$ and $(\hat{f}_{r4} - f_{r4})$, respectively. The gain k_1 is selected to satisfy the

following sliding condition:

$$\frac{1}{2}\frac{\mathrm{d}}{\mathrm{d}t}s_{\mathrm{ob}}^2(\underset{\sim}{\tilde{x}},t)\leqslant-\eta_{\mathrm{ob}}|s_{\mathrm{ob}}|\Rightarrow k_1\geqslant\eta_{\mathrm{ob}}-\bar{k}_1|\tilde{x}_{r1}|+\tilde{x}_{r3}\,\mathrm{sgn}(\tilde{x}_{r1}). \tag{32}$$

In addition, k_1 must be positive so that the switching term, $-k_1\,\mathrm{sgn}(\tilde{x}_{r1})$, can force the system to remain on the sliding surface in the presence of both model imprecision and disturbances. Therefore, Eq. (32) has been modified to yield

$$k_1\geqslant\eta_{\mathrm{ob}}+|\bar{k}_1\tilde{x}_{r1}|+|\tilde{x}_{r3}|, \tag{33}$$

when the system is located on the sliding surface, its dynamics are governed by

$$\dot{s}_{\mathrm{ob}}=C[\Delta\underset{\sim}{f}_r-\bar{k}\tilde{x}_{r1}-k\,\mathrm{sgn}(\tilde{x}_{r1})]=0. \tag{34}$$

Note that only θ is considered herein to be known through measurements. Thus, the C matrix can be defined as $[1\quad 0\quad 0\quad 0]$. Due to disturbances and model uncertainties, the system may leave the sliding surface; thus, causing $\tilde{x}_{r1}$ to become different than zero. It should be emphasized that the $\bar{k}$ term in the above equation represents the Luenberger observer gain matrix. It has been introduced in this formulation to aid the system in reaching the sliding surface. However, when the system is in the sliding mode, $\bar{k}\tilde{x}_{r1}$ becomes negligible due to the small numerical values of $\tilde{x}_{r1}$. The robustness of the system is ensured by the switching term $k\,\mathrm{sgn}(\tilde{x}_{r1})$, which forces the system to return to the sliding surface whenever $\tilde{x}_{r1}$ becomes different than zero. Based on this reason, the $\bar{k}\tilde{x}_{r1}$ term has been ignored in the computation of $\mathrm{sgn}(\tilde{x}_{r1})$. Therefore, the switching term is determined from Eq. (34) as follows:

$$\mathrm{sgn}(\tilde{x}_{r1})=(Ck)^{-1}C\Delta\underset{\sim}{f}_r. \tag{35}$$

Combining Eqs. (31) and (35), the error vector equation becomes

$$\begin{aligned}\dot{\underset{\sim}{\tilde{x}}}_r&=(I-k(Ck)^{-1}C)\Delta\underset{\sim}{f}_r\\&=\begin{pmatrix}0&0&0&0\\-\frac{k_2}{k_1}&1&0&0\\-\frac{k_3}{k_1}&0&1&0\\-\frac{k_4}{k_1}&0&0&1\end{pmatrix}\Delta\underset{\sim}{f}_r=\begin{pmatrix}0&0&0&0\\0&0&-\frac{k_2}{k_1}&1\\0&0&-\frac{k_3}{k_1}&0\\0&0&-\frac{k_4}{k_1}&0\end{pmatrix}\underset{\sim}{\tilde{x}}_r+\begin{pmatrix}0&0\\0&0\\1&0\\0&1\end{pmatrix}\begin{Bmatrix}\Delta f_{r3}\\\Delta f_{r4}\end{Bmatrix}.\end{aligned} \tag{36}$$

For an asymptotically stable response of the homogeneous part of the $\tilde{x}_{r3}$ differential equation, k_3/k_1 must be positive. However, according to Eq. (33), k_1 can only take on positive numerical values; thus, causing k_3 to be positive.

Due to the unavailability of $\tilde{x}_{r2}$, $\tilde{x}_{r3}$ and $\tilde{x}_{r4}$, a feedforward compensation is implemented herein based on upper bounds of modeling uncertainties and error variables. For instance, in the computation of k_1 as defined by Eq. (33), both η_{ob} and $\bar{k}_1$ are considered to be known quantities because they are assigned by the designer. Moreover, $\tilde{x}_{r1}$ is available through direct measurement. The remaining unknown term $\tilde{x}_{r3}$ is selected to be the desired upper bound of the error in the estimation of x_{r3}. This yields the following expression for k_1:

$$k_{1\text{upper\_bound}} \geqslant \eta_{ob} + |\bar{k}_1 \tilde{x}_{r1}| + |\tilde{x}_{r3}|_{\text{desired upper\_bound}}. \tag{37}$$

Similarly, k_2, k_3 and k_4 are determined as follows:

$$k_{2\text{upper\_bound}} = k_{1\text{upper\_bound}} \frac{\text{Educated guess on } (\tilde{x}_{r4})_{\max}}{(\tilde{x}_{r3})_{\text{desired upper\_bound}}}, \tag{38a}$$

$$k_{3\text{upper\_bound}} = k_{1\text{upper\_bound}} \frac{\text{upper bound on } \Delta f_{r3}}{(\tilde{x}_{r3})_{\text{desired upper\_bound}}}, \tag{38b}$$

$$k_{4\text{upper\_bound}} = k_{1\text{upper\_bound}} \frac{\text{upper bound on } \Delta f_{r4}}{(\tilde{x}_{r3})_{\text{desired upper\_bound}}}. \tag{38c}$$

Note that $\bar{k}$, representing the Luenberger observer gain matrix, has been treated thus far as a known quantity. It is determined based on the $\bar{A}$ and $\bar{C}$ matrices obtained by linearizing Eq. (8) around $\underset{\sim}{\hat{x}}_{re} = \underset{\sim}{0}$. It is computed herein by assigning $\lambda_1 = -10$, $\lambda_2 = -11$, $\lambda_3 = -12$ and $\lambda_4 = -13$ as the desired eigenvalues for the $(\bar{A} - \bar{k}\,\bar{C})$ matrix. It should be stressed that the $\bar{k}\,\tilde{x}_{r1}$ term provides additional corrective action that aids the system in reaching the sliding surface.

The preliminary results have demonstrated that the above observer suffers from unacceptable errors whenever the actual and estimated state vectors have different initial conditions. To alleviate this problem, Eqs. (30b)–(30d) have been modified by introducing a feedback loop based on the estimated state variables as follows:

$$\dot{\hat{x}}_{r2} = \hat{x}_{r4} - \bar{k}_2 \tilde{x}_{r1} - k_2 \operatorname{sgn}(\tilde{x}_{r1}) - \overline{\overline{k_2}} \hat{x}_{r2}, \tag{39a}$$

$$\dot{\hat{x}}_{r3} = \hat{f}_{r3}(\underset{\sim}{\hat{x}}_r, \tau_1) - \bar{k}_3 \tilde{x}_{r1} - k_3 \operatorname{sgn}(\tilde{x}_{r1}) - \overline{\overline{k_3}} \hat{x}_{r3}, \tag{39b}$$

$$\dot{\hat{x}}_{r4} = \hat{f}_{r4}(\underset{\sim}{\hat{x}}_r, \tau_1) - \bar{k}_4 \tilde{x}_{r1} - k_4 \operatorname{sgn}(\tilde{x}_{r1}) - \overline{\overline{k_4}} \hat{x}_{r4}, \tag{39c}$$

where $\overline{\overline{k}}_2$, $\overline{\overline{k}}_3$ and $\overline{\overline{k}}_4$ have been selected to yield eigenvalues with negative real parts for the homogeneous parts of Eqs. (39a)–(39c). Their numerical values were fine tuned to yield the best compromise between the convergence rate and the estimation errors. Note that large numerical values of $\overline{\overline{k}}_i$'s have had a tendency to increase the convergence rate of the observer at the expense of deteriorating the estimation accuracy.

Table 3
Numerical values of the system parameters

Parameters of the physical system	Value
Cross sectional area of the beam (A)	7.2839×10^{-4} m^2
Outer radius of the beam (R_o)	0.0381 m
Inner radius of the beam (R_i)	0.0349 m
Length of the beam (L)	2.3 m
Density of aluminum (ρ)	2707 kg/m^3
Mass of the beam (M_B)	4.535 kg
Payload mass (m_p)	3.405 kg

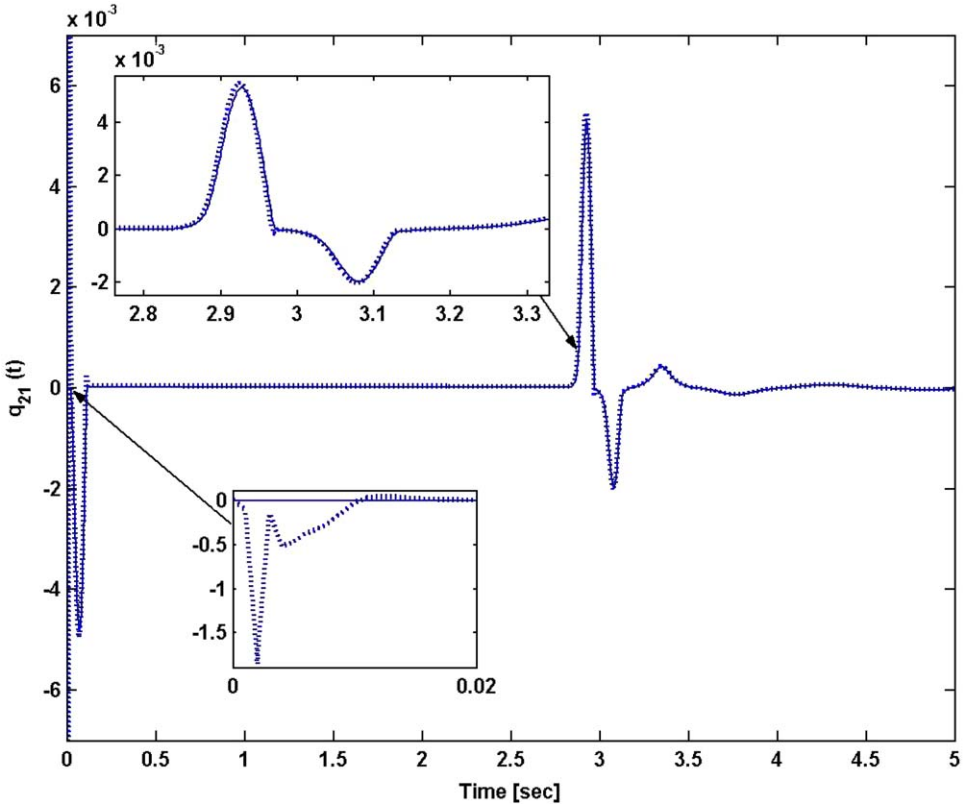

Fig. 4. Estimated (……) and actual (——) generalized coordinate q_{21} when the plant is controlled by CSMC.

5. Performance assessment of the controllers and the observer

The dynamic model, accounting for two elastic modes of the flexible link and derived in Section 2, is used herein as a test bed to assess the combined performances of the controllers and the observer in controlling the rigid and flexible motions of the robotic manipulator. The digital simulations are carried out based on the numerical values of the model parameters listed in Table 3.

The observer gains are selected to be $\bar{k} = [46 \quad 55.606 \quad 155791 \quad 188164]$ and $\bar{\bar{k}} = [10 \quad 10 \quad 10]$. It is being used herein to provide on-line estimates for θ, q_{21}, $\dot{\theta}$ and $\dot{q}_{21}$, which are needed for the computation of the control signals of both CSMC and FSMC.

The performance criteria for the controllers are based on achieving zero steady-state error in θ, damping out the unwanted vibrations of the beam, and avoiding excessive control torque requirements. The η and λ parameters of the CSMC have been selected to be 11 and 40, respectively. These values were found to yield the best compromise between the reaching time, t_{reach}, the minimum overshoot in θ and the minimum deformations of the beam.

First, the combined performances of the controllers and the observer are assessed in the presence of structured uncertainties of the system. This is done in this study by implementing the controllers and the observer on the simplified version of the model of the plant, which only takes

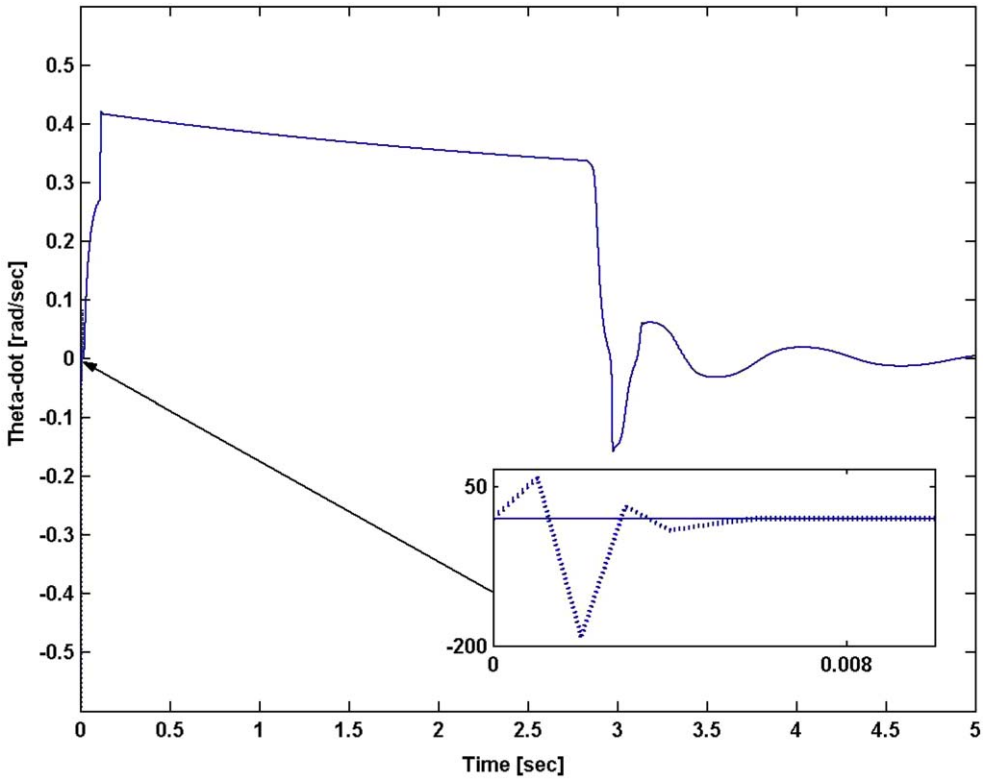

Fig. 5. Estimated (……) and actual (——) $\dot{\theta}$ when the plant is controlled by CSMC.

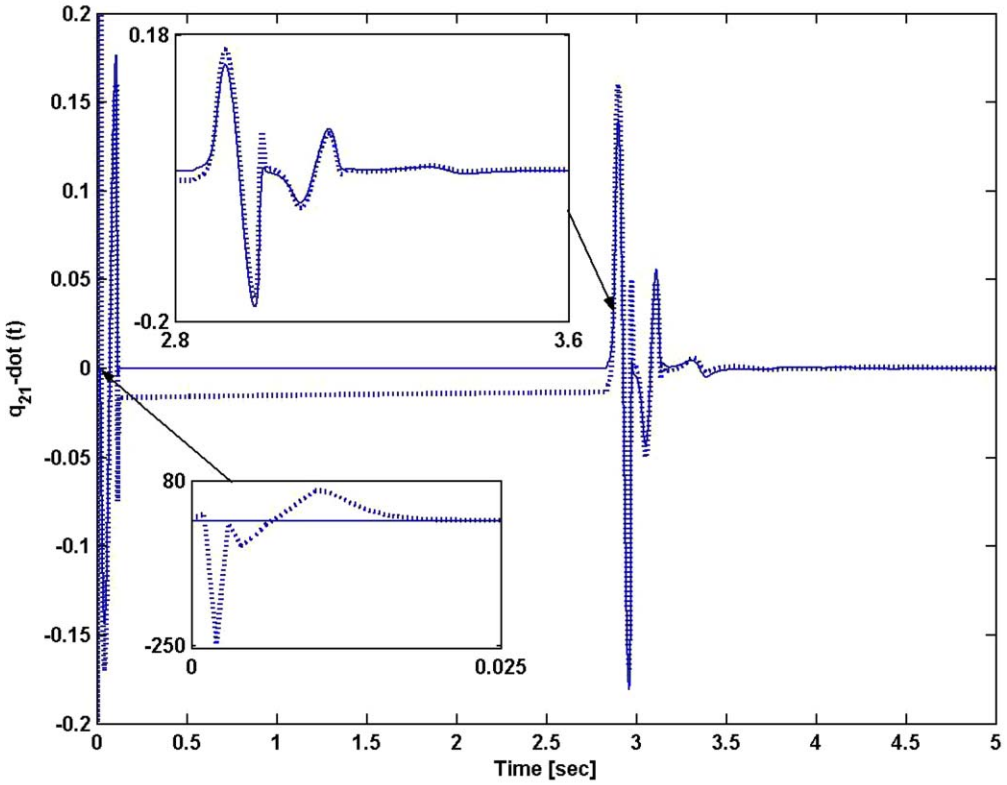

Fig. 6. Estimated (……) and actual (——) $\dot{q}_{21}$ when the plant is controlled by CSMC.

into consideration the first elastic mode of the beam. The initial conditions for the state vectors of both the plant and the observer are defined to be $x_r(0) = 0$ and $\hat{x}_r(0) = [0.1 \quad 0.004 \quad 0.2 \quad 0.5]^T$, respectively. The performance of the observer, when the robot arm is controlled by the CSMC and FSMC, is illustrated in Figs. 4–8. Note that only the state variables with the most errors in their estimations are shown here due to the limited space. The results demonstrate the capability of the nonlinear observer in accurately estimating the state variables in the presence of structured uncertainties of the system. Note that $\dot{q}_{21}$ has the slowest convergence rate among all the state variables (see Figs. 6 and 8).

A closer look at the results reveals that all the estimated state variables suffer from very large errors during the initial period between $t = 0$ and 0.02 s. These errors stem from the difference in the initial conditions between the plant and the observer. The large magnitudes of these errors have rendered the estimated state variables to be unacceptable for the computation of the control signals during the period between $t = 0$ and 0.02 s. Therefore, all the digital simulations, performed in the current work, have been carried out by activating the controllers at $t = 0.02$ s. This allows the estimation errors to become within an acceptable range before the estimated state variables can be used in the computation of the control signals. Note that the proposed delay in

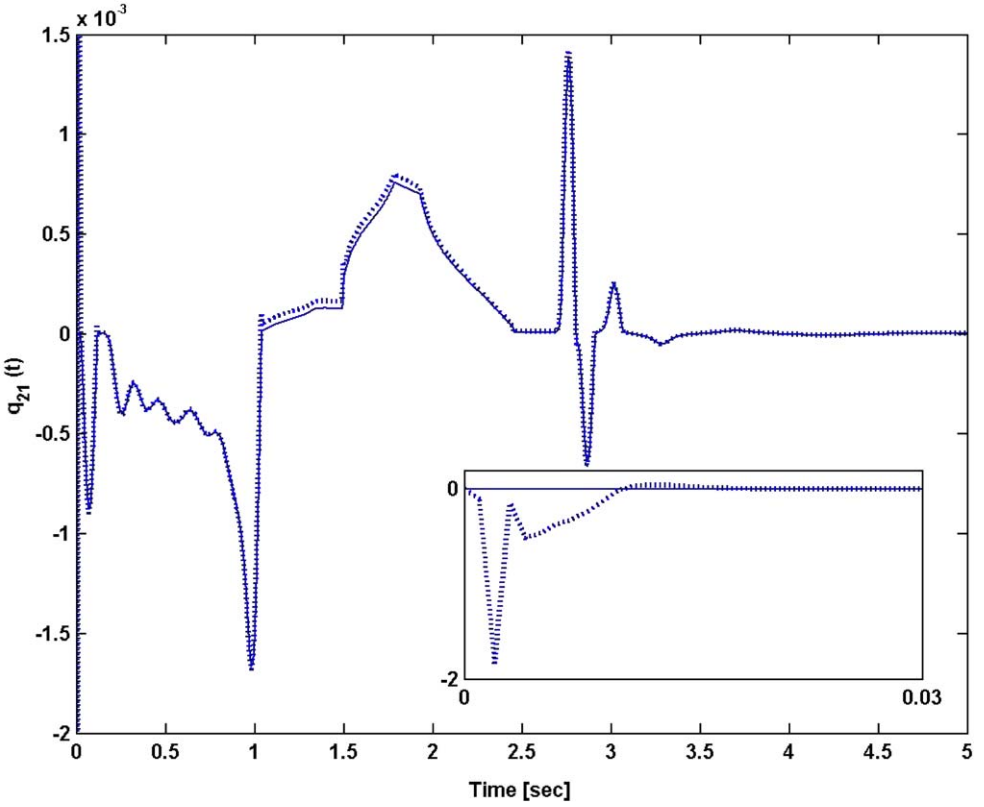

Fig. 7. Estimated (.....) and actual (——) q_{21} when the plant is controlled by FSMC.

activating the controller spans over the first few sampling periods and has a minimal effect on the time constant of the closed-loop system.

The performance of the CSMC, with or without the observer, is shown in Figs. 9a–11a. The settling time for θ, based on a 2% criterion, is $\cong 2.7$ s (see Fig. 9a). Note that the system has reached its target with a large momentum and with a sharp angle of approach. This is due to the inability of the CSMC to exert a negative control torque in order to slow down the system response prior to reaching its target. As a consequence, the system response became highly oscillatory inside the boundary layer; thus, causing the beam to undergo large deformations around $t = 2.7$ s (see Fig. 10a). Furthermore, the "whiplash" effect is exhibited by the large structural deformations at the beginning of the beam movement. It should be pointed out that the magnitude of the "whiplash" deformation is strongly influenced by the choice of η, which is dictated by many factors such as the system overshoot, t_{reach} and the "whiplash" induced deformations. Thus, it is extremely hard to effectively reduce the initial spikes in the deformation curve in the case of CSMC, which uses constant numerical values for both η and λ. Moreover, Figs. 9a–11a reveal no deterioration in the closed-loop system response by computing the control actions based on estimated rather than actual state variables. In fact, the

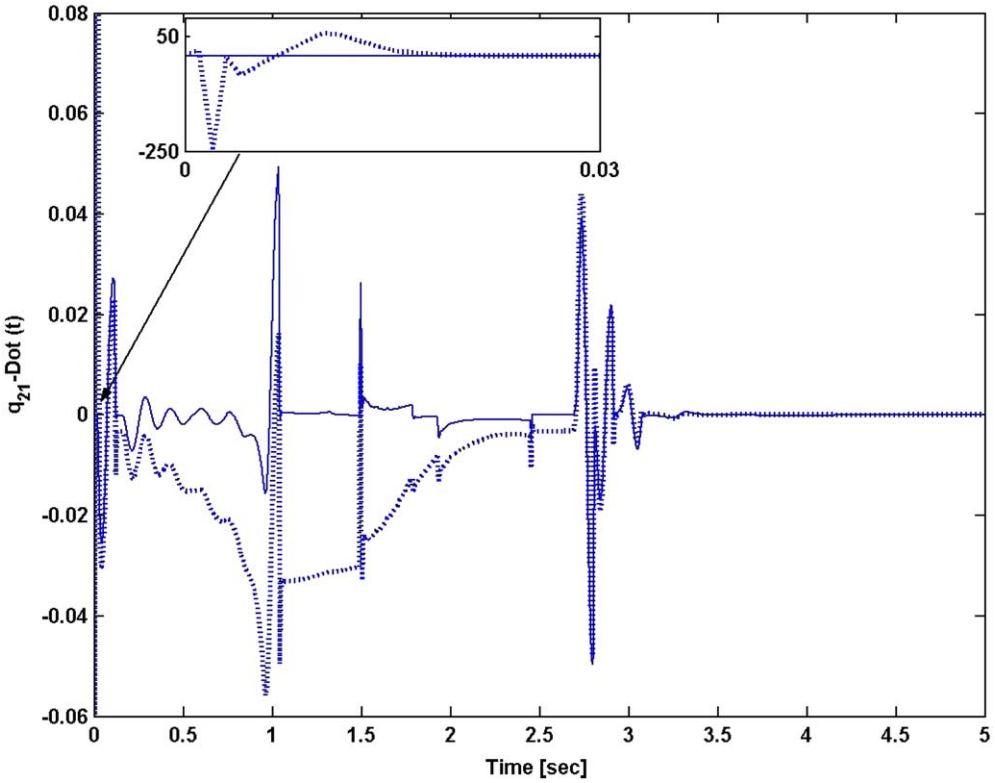

Fig. 8. Estimated (.....) and actual (——) $\dot{q}_{21}$ when the plant is controlled by FSMC.

beam has experienced a smaller deformation around $t = 2.7$ s when the estimated state variables were used. Moreover, the slight shift in the control signal, exhibited in Fig. 11a, is attributed to the additional system uncertainties brought about by the errors in the estimation of the state variables. As a result, the beam deformation curve has experienced a similar shift. This is illustrated in Fig. 10a.

Next, the performance of the FSMC is assessed. Note that this controller has the capability of providing a negative control torque in the region prior to reaching the sliding surface. Fig. 9 shows that the FSMC yields a totally different transient response for θ than the one generated by the CSMC. The lower portion of the S-shaped θ response is due to fuzzy-tuning η, which helped in significantly reducing the "whiplash" effect deformations of the beam (see Fig. 10b). On the other hand, the upper portion of the S-shaped response stems from the negative control torque applied by the FSMC to dissipate the momentum of the system as it approaches its final destination. It should be emphasized that both FSMC and CSMC have led to the same settling time for θ (see Fig. 9). Furthermore, the closed-loop system response generated by the CSMC exhibits larger oscillations than the one obtained by the FSMC (see Fig. 9). This is because the FSMC boundary layer thickness is much smaller than the one corresponding to the CSMC; thus, leading to a more accurate beam response by the FSMC than

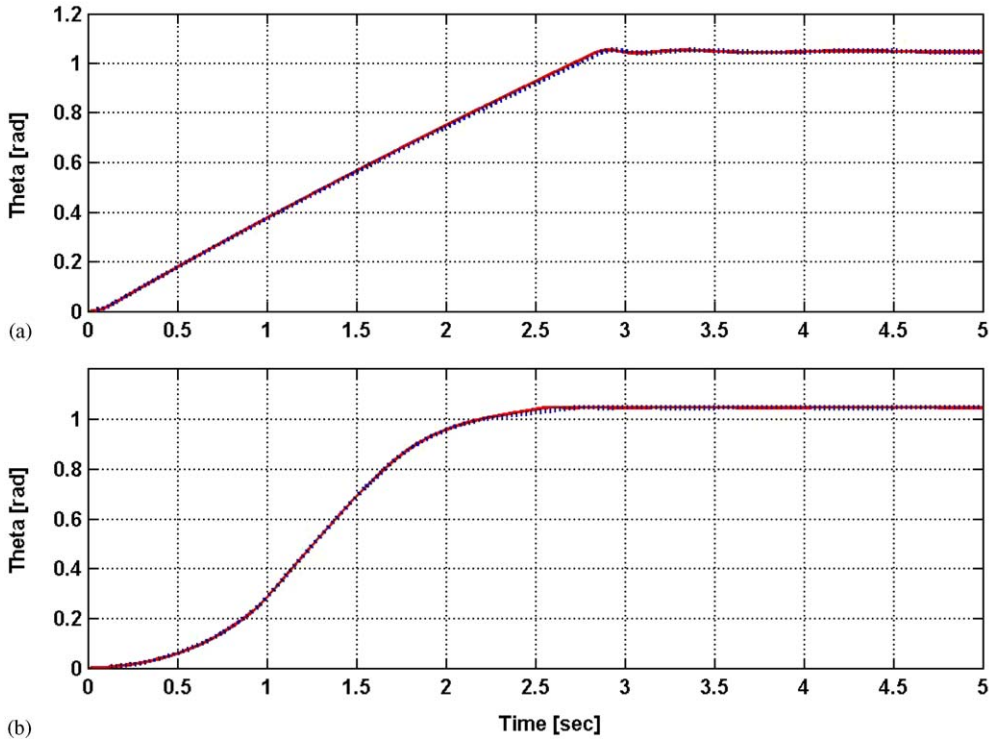

Fig. 9. Controlled θ-response: (a) Generated by using the CSMC with (.....) or without (——) the observer, (b) generated by using the FSMC with (.....) or without (——) the observer.

by the CSMC. Moreover, Fig. 10 demonstrates that the performance of the FSMC is far more superior to that of the CSMC in damping out the unwanted vibrations of the beam. The absolute maximum deformations at the free-end of the beam are found to be 10.8 and 4.08 mm for the CSMC and FSMC cases, respectively. In addition, Fig. 11 shows that the maximum control torques required by the CSMC and FSMC to be -232 and -87.4 N m, respectively. This demonstrates that the proposed FSMC requires a significantly smaller control torque at the base joint of the flexible beam than the CSMC. Moreover, Figs. 9b–11b actually illustrate some improvement in the closed-loop system response when the estimated rather than the actual state variables are used in the computation of the control signals. Furthermore, the shift in the control signal, due to the uncertainties that are induced by the estimation errors, is more pronounced in the FSMC case than in the CSMC one (see Fig. 11). This is due to the stronger impact that these uncertainties have had on the FSMC control strategy, particularly during the period when the brake torque is applied. Consequently, the deformation curve experienced a similar shift (see Fig. 10b).

Second, the combined performances of the controllers and the observer are examined in the presence of both structured and unstructured uncertainties. This is done by considering the test bed to be the dynamic model of the manipulator that accounts for the first two elastic modes of the link. Note that the simplified version of the robot model, which only

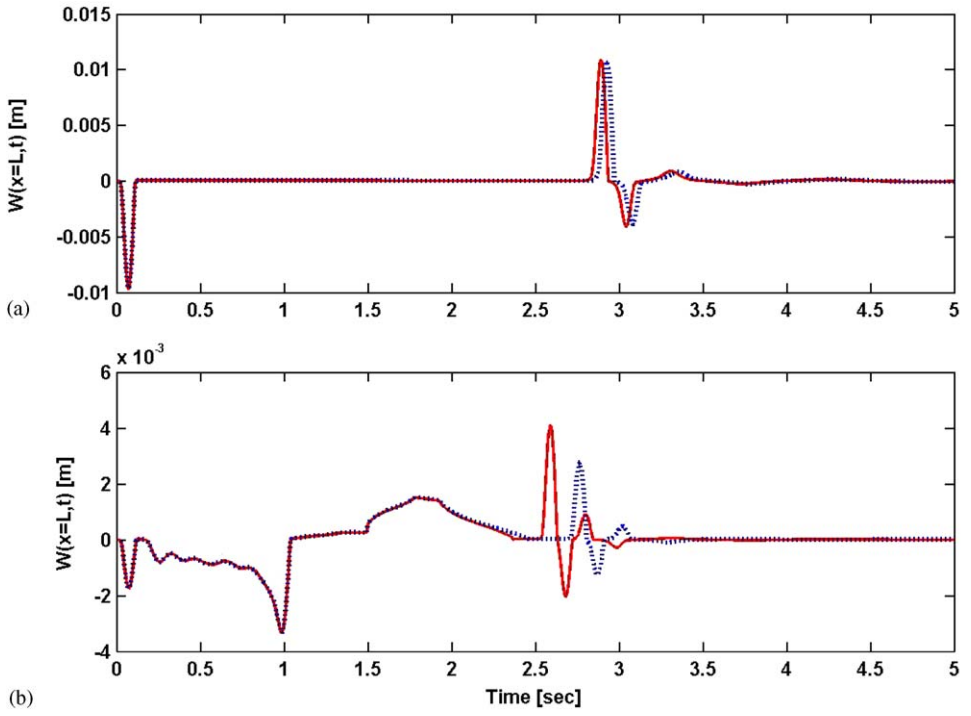

Fig. 10. Deformation at the free-end of the beam: (a) Obtained by applying the CSMC with (……) or without (——) the observer, (b) obtained by applying the FSMC with (……) or without (——) the observer.

accounts for the first elastic mode of the beam, is used herein for the purpose of designing the controllers and the observer. The results, shown in Figs. 12–14, reveal the same pattern of the closed-loop response as the one observed in Figs. 9–11. The absolute maximum deformations at the free-end of the beam are found to be 14.4 and 3.36 mm for the CSMC and FSMC cases, respectively. In addition, Fig. 14 shows that the maximum control torques required by the CSMC and FSMC are -305 and -71 N m, respectively. Therefore, the unstructured uncertainties, associated with the second elastic mode of the plant, have had an adverse effect on the CSMC performance and a favorable effect on the FSMC performance. These results have confirmed the capability of the proposed controllers and observer to yield a desired response of the plant in the presence of both structured and unstructured uncertainties.

6. Summary and conclusions

Two robust nonlinear controllers along with a nonlinear observer have been developed in this study to control the rigid and flexible motions of a single-link robotic manipulator. The dynamic model of the robot arm is developed by taking into consideration the rigid-body

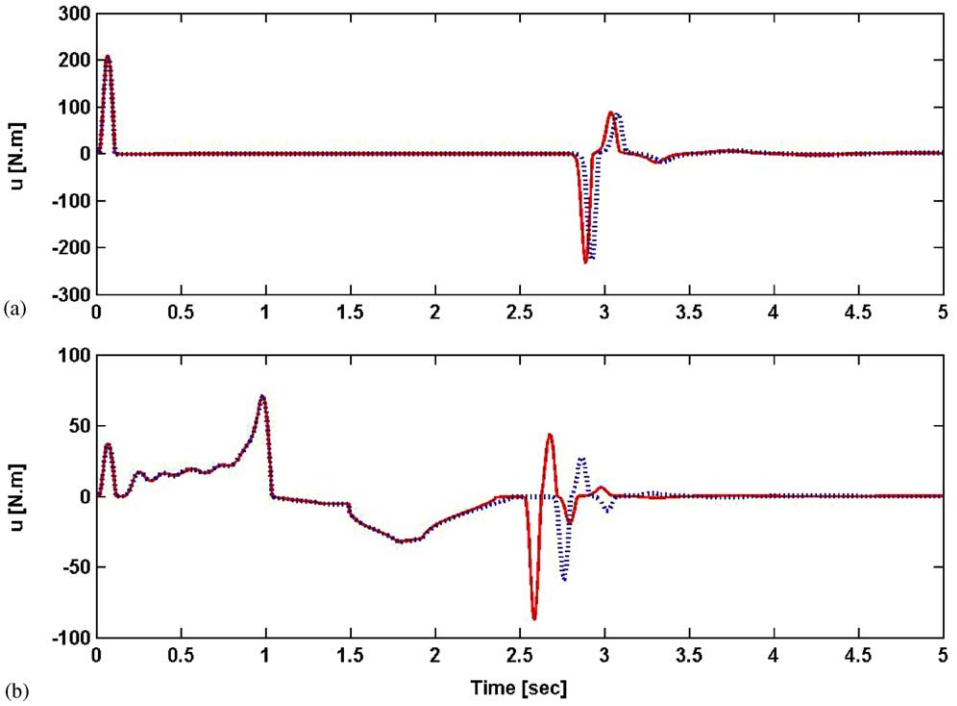

Fig. 11. Control torque at the base joint: (a) Generated by applying the CSMC with (.....) or without (——) the observer, (b) generated by applying the FSMC with (.....) or without (——) the observer.

motion of the link along with its in-plane transverse deformation. The payload is treated as a point mass located at the free-end of the beam. The assumed modes method is implemented to approximate the transverse deflection, which is assumed to be dominated by the first two elastic modes. Note that the second elastic mode is included in the model to investigate the effects of unstructured uncertainties on the overall performance of the closed-loop system.

The controllers and the observer have been designed in this study based on a simplified version of the model of the arm, which only accounts for the first elastic mode of the link. The controllers consist of a CSMC and an FSMC. The FSMC, whose parameters are determined by FIS, has been designed based on two Lyapunov functions. The rationale is to provide the FSMC with the capability of exerting negative control torque during the period when the system is approaching the boundary layer neighboring the sliding surface. This will significantly reduce the momentum with which the system approaches the boundary layer; thus, resulting in considerably smaller structural deformations of the system.

Moreover, the robust nonlinear observer has been designed based on the sliding mode methodology. It is implemented herein to estimate θ, q_{21}, $\dot{\theta}$, and $\dot{q}_{21}$.

The digital simulations have demonstrated the capability of the observer in yielding accurate estimates of the state variables in the presence of modeling uncertainties. It has been successfully

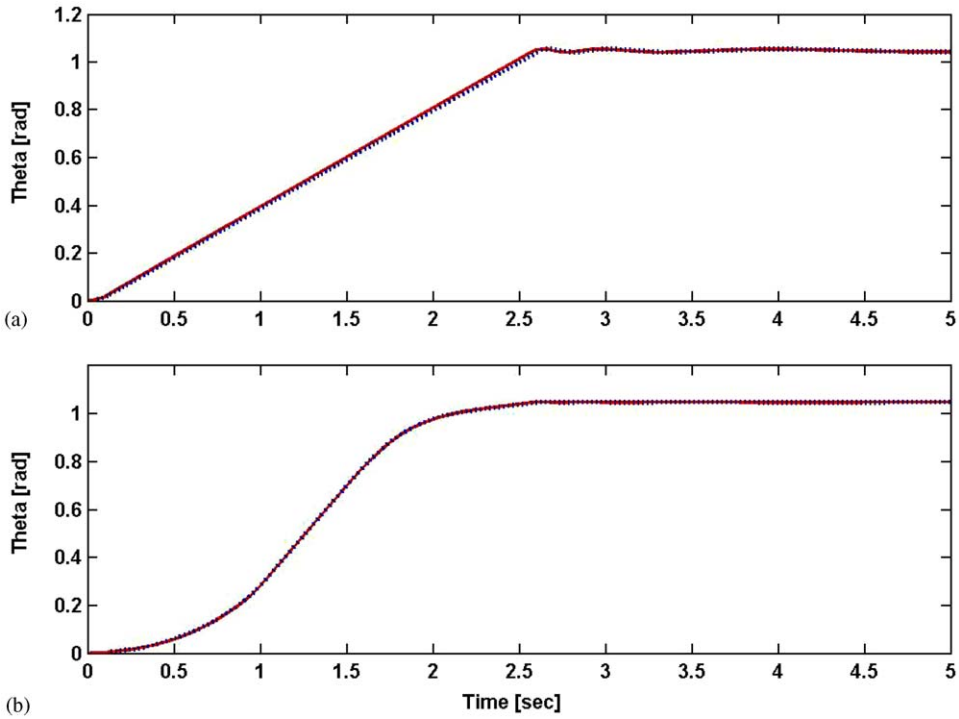

Fig. 12. Controlled θ-response: (a) Generated by using the CSMC with (.....) or without (——) the observer, (b) generated by using the FSMC with (.....) or without (——) the observer.

implemented to provide on-line estimates of the state variables for the computation of the control signals. The results have illustrated robust performances of the controllers and the observer in controlling the rigid and flexible motions of the manipulator in the presence of both structured and unstructured uncertainties. This was achieved irrespective of the differences in the initial conditions between the plant and the observer. Moreover, the reliance on estimated rather than actual state variables in the computation of the control signals has been shown to enhance the suppression of the unwanted vibrations of the arm.

Furthermore, the structural deformations, incurred by the beam at the onset of its movement, have been shown to be significantly reduced by fuzzy-tuning the η-control parameter. The results have illustrated the superiority of the FSMC over the CSMC in producing less oscillatory and more accurate response of the angular displacement at the base joint, in damping out the unwanted vibrations of the beam, and in requiring significantly smaller control torques.

Future steps will include experimental work to validate the combined performances of the controllers and the observer. Among the challenges to be encountered are the impact of measurement noise on the performance of the observer and the effect of sampling rate on the performance of the closed-loop system.

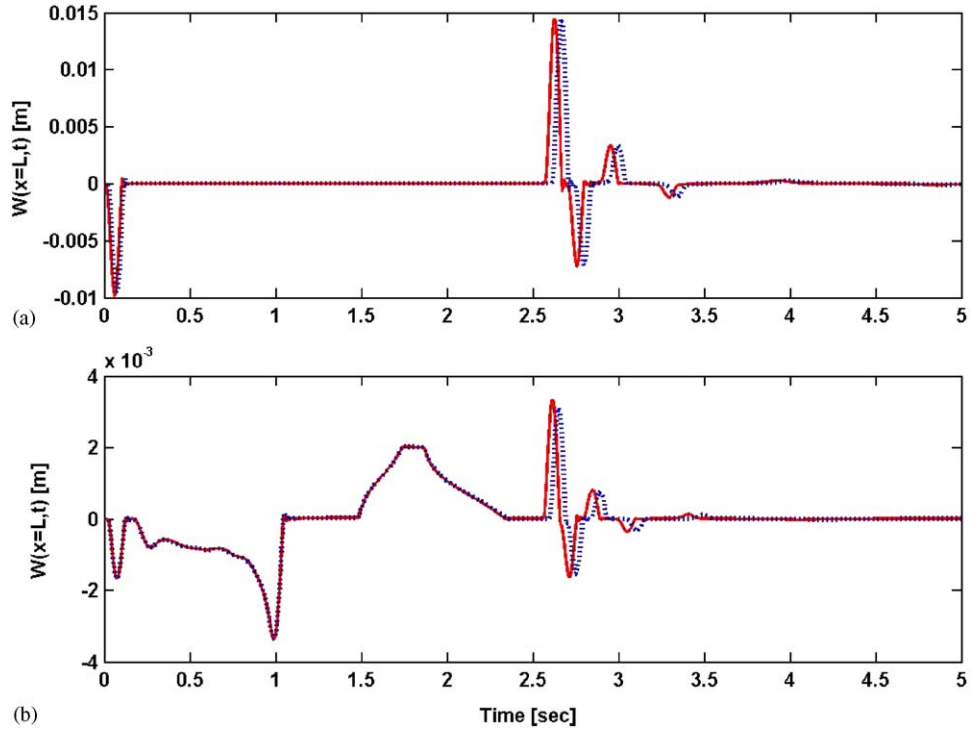

Fig. 13. Deformation at the free-end of the beam: (a) Obtained by applying the CSMC with (.....) or without (——) the observer, (b) obtained by applying the FSMC with (.....) or without (——) the observer.

Appendix A. Expressions for $\ddot{\theta}$ and $\ddot{q}_{21}$ in the simplified version of the model

The detailed expressions for $\ddot{\theta}$ and $\ddot{q}_{21}$ are:

$$\ddot{\theta} = f_{r3}(\underset{\sim}{x_r}, \tau_1) = g_{r1}(\underset{\sim}{x_r}) + b_1(\underset{\sim}{x_r})\tau_1$$

$$= -\frac{x_{r2}(661.69x_{r3}x_{r4} - 66.85x_{r3}^2 - 772189)}{330.85x_{r2}^2 + 5.86} + \frac{18.19\tau_1}{330.85x_{r2}^2 + 5.86},$$

$$\ddot{q}_{21} = f_{r4}(\underset{\sim}{x_r}, \tau_1) = g_{r2}(\underset{\sim}{x_r}) + b_2(\underset{\sim}{x_r})\tau_1$$

$$= -\frac{x_{r2}(930210 - 787.26x_{r3}x_{r4} + 80.53x_{r3}^2 + 649027x_{r2}^2 + 56.19x_{r2}^2x_{r3}^2)}{330.85x_{r2}^2 + 5.86}$$

$$-\frac{21.64\tau_1}{330.85x_{r2}^2 + 5.86}.$$

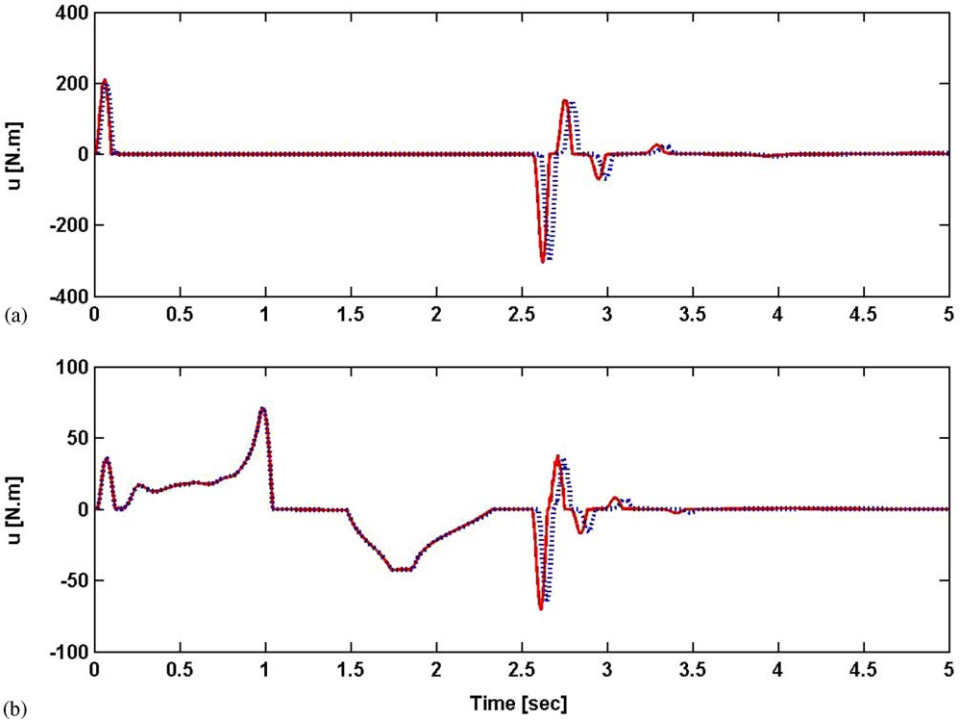

Fig. 14. Control torque at the base joint: (a) Generated by applying the CSMC with (……) or without (——) the observer, (b) generated by applying the FSMC with (……) or without (——) the observer.

References

[1] W.J. Book, O. Maizza-Neto, D.E. Whitney, Feedback control of two beams, two joint systems with distributed flexibility, *ASME Journal of Dynamic Systems, Measurement and Control* 97 (1975) 424–431.

[2] N.G. Chalhoub, A.G. Ulsoy, Dynamic simulation of a leadscrew driven flexible robot arm and controller, *ASME Journal of Dynamic Systems, Measurement and Control* 108 (1986) 119–126.

[3] N.G. Chalhoub, X. Zhang, Reduction of the end effector sensitivity to the structural deflections of a single flexible link: theoretical and experimental results, *ASME Journal of Dynamic Systems, Measurement and Control* 115 (1993) 658–666.

[4] L. Chen, N.G. Chalhoub, Modeling and control of transverse and torsional vibrations in a spherical robotic manipulator: theoretical and experimental results, *ASME Journal of Dynamic Systems, Measurement and Control* 119 (1997) 421–430.

[5] S.N. Singh, A.A. Schy, Decomposition and state variable feedback control of elastic robotic systems, *in: Proceedings of the 1985 ACC* 2 (1985) 375–380.

[6] J.J.E. Slotine, W. Li, *Applied Nonlinear Control*, Prentice-Hall, Englewood Cliffs, NJ, 1991.

[7] H.K. Khalil, *Nonlinear Systems*, second ed, Prentice-Hall, Englewood Cliffs, NJ, 1996.

[8] H. Lee, E. Kim, H.J. Kang, M. Park, A new sliding-mode control with fuzzy boundary layer, *Fuzzy Sets and Systems* 120 (2001) 135–143.

[9] J.J. Slotine, S.S. Sastry, Tracking control of non-linear systems using sliding surfaces, with application to robot manipulators, *International Journal of Control* 38 (1983) 465–492.

[10] S.B. Choi, J.S. Kim, A fuzzy-sliding mode controller for robust tracking of robotic manipulators, *Mechatronics* 7 (1997) 199–216.
[11] S.B. Choi, D.W. Park, Moving sliding surfaces for fast tracking control of second-order dynamical systems, *Journal of Dynamic Systems, Measurement, and Control* 116 (1994) 154–158.
[12] Q.P. Ha, D.C. Rye, H.F. Durrant-Whyte, Fuzzy moving sliding mode control with application to robotic manipulators, *Automatica* 35 (1999) 607–616.
[13] S.B. Choi, C.C. Cheong, H.C. Shin, Sliding mode control of vibration in a single-link flexible arm with parameter variations, *Journal of Sound and Vibration* 179 (1995) 737–748.
[14] W.T. Qian, C.C.H. Ma, A new controller design for a flexible one-link manipulator, *IEEE Transactions on Automatic Control* 37 (1992) 132–137.
[15] M. Gokasan, O.S. Bogosyan, A. Arabyan, A. Sabanovic, A sliding mode based controller for a flexible arm with a load, *IEEE Transactions* (1998) 1083–1087.
[16] S.B. Choi, D.W. Park, S. Jayasuriya, A time-varying sliding surface for fast and robust tracking control of second-order uncertain systems, *Automatica* 30 (1994) 899–904.
[17] A. Bartoszewicz, A comment on a 'a time-varying sliding surface for fast and robust tracking control of second-order uncertain systems', *Automatica* 31 (1995) 1893–1895.
[18] M.H. Kim, D.J. Inman, Reduction of observation spillover in vibration suppression using a sliding mode observer, *Journal of Vibration and Control* 7 (2001) 1087–1105.
[19] B.L. Walcott, S.H. Zak, Observation of dynamical systems in the presence of bounded nonlinearities/uncertainties, in: *Proceedings of the 25th Conference on Decision and Control*, Athens, Greece, 1986.
[20] J.J.E. Slotine, J.K. Hedrick, E.A. Misawa, On sliding observers for nonlinear systems, *Journal of Dynamic Systems, Measurement, and Control* 109 (1987) 245–252.
[21] E.A. Misawa, J.K. Hedrick, Nonlinear observers—a state-of-the-art survey, *Journal of Dynamic Systems, Measurement, and Control* 111 (1989) 344–352.
[22] J. Wagner, R. Shoureshi, Observer designs for diagnostics of nonlinear processes and systems, *ASME Winter Annual Meeting*, 88-WA/DSC-5, 1988.
[23] W. Baumann, W. Rugh, Feedback control of non-linear systems by extended linearization, *IEEE Transactions on Automatic Control* AC-31 (1986) 40–47.
[24] F.E. Thau, Observing the state of non-linear dynamic systems, *International Journal of Control* 17 (1973) 471–479.
[25] C. Canudas De Wit, J.-J.E. Slotine, Sliding observers for robot manipulators, *Automatica* 27 (1991) 859–864.
[26] L. Meirovitch, *Analytical Methods in Vibrations*, Macmillan, New York, 1967.
[27] D. Young, R.P. Felgar, *Tables of Characteristic Functions Representing Normal Modes of Vibration of a Beam*, The University of Texas, Publication 4913, 1949.
[28] J.C. Simo, L. Vu-Quoc, The role of non-linear theories in transient dynamic analysis of flexible structures, *Journal of Sound and Vibration* 119 (1987) 487–508.
[29] C.W. Gear, *Numerical Initial Value Problems in Ordinary Differential Equations*, Prentice-Hall, Englewood Cliffs, NJ, 1971.